科学通报 2026 年 第 71 卷 第 32 期: 7314 ~ 7324
厦门大学海洋学系建系80周年专辑 进 展
《中国科学》杂志社 SCIENCE CHINA PRESS

海洋多尺度动力分解新理论与方法

王传印[1], 刘志宇[2*], 林宏阳[2], 杨清华[1,3], 倪钦彪[1], 陈大可[1,4]

1. 南方海洋科学与工程广东省实验室(珠海), 珠海 519082
2. 海洋生物地球化学全国重点实验室, 厦门大学海洋与地球学院, 厦门 361102
3. 中山大学大气科学学院, 珠海 519082
4. 自然资源部第二海洋研究所, 卫星海洋环境监测预警全国重点实验室, 杭州 310012
* 联系人, E-mail: zyliu@xmu.edu.cn

2025-09-22 收稿, 2025-11-11 修回, 2025-11-24 接受, 2025-11-28 网络版发表
国家重点研发计划(2023YFF0805502, 2022YFA1003804, 2023YFC3107802, 2023YFE0126700)和国家自然科学基金(42406021, 92258301)资助

摘要 海洋多尺度相互作用是物理海洋学的重要研究前沿, 多尺度运动分解是揭示多尺度相互作用机理与量化跨尺度能量传递的关键. 目前学界普遍采用的多尺度运动分解方法本质上是基于时间或空间尺度的分解, 因此无法准确分离时空尺度相近、但动力属性迥异的运动过程, 这严重制约了海洋多尺度相互作用理论的发展. 本文简要总结近年来我们在海洋多尺度运动分解方面取得的进展: 针对基于高分辨数值模拟数据的多尺度相互作用机理研究需要, 提出了连续时间物理场中平衡运动(包括大尺度环流、中尺度流动、亚中尺度过程)与非平衡运动(包括正压潮、内波)的动力分解理论与方法, 并导出了两类运动的控制方程; 针对可分辨亚中尺度的SWOT(Surface Water and Ocean Topography)卫星数据定量化科学应用的需要, 参照数值天气预报中的初始化问题, 通过额外引进海表面流场数据, 利用内波不携带位势涡度异常这一地球物理流体力学基本性质, 建立了由瞬时海面高度场中分解出平衡运动与非平衡运动的方法. 该系列工作为海洋多尺度相互作用机理研究与SWOT卫星数据的科学应用奠定了理论与方法学基础.

关键词 动力分解, 多尺度相互作用, 平衡运动, 非平衡运动, SWOT

海洋是一个高度复杂的动力系统, 蕴含多种运动过程, 时空尺度跨越多个数量级. 海洋多尺度运动主要分为平衡运动和非平衡运动两大类. 平衡运动是指携带位势涡度的运动, 包括大尺度环流、中尺度流动和亚中尺度过程等; 非平衡运动是指不携带位势涡度的运动, 主要包括正压潮和内波. 如《中国海洋科学2035发展战略》所指出的, 海洋多尺度动力学是当前海洋科学的重要前沿[1]. 围绕这一研究方向, 中国国家自然科学基金委员会部署了“西太平洋地球系统多圈层相互作用”重大研究计划, 经费达2亿元人民币, 实施周期为2019~2026年(http://www.wespmi.ac.cn/web/hm/index); 德国科学基金会设立了“Energy Transfers in Atmosphere and Ocean”协同研究中心, 经费达0.36亿欧元, 实施周期为2016~2028年(https://www.trr-energy-transfers.de/). 这些举措旨在揭示海洋多尺度动力过程的特征与机理, 厘清海洋平衡运动和非平衡运动相互作用及其所致能量传递的规律, 发展满足能量守恒约束的海洋数值模型, 引领跨尺度系统性研究.

近十余年来, 海洋高分辨率数值模拟和新型观测技术的迅猛发展为海洋多尺度动力学研究提供了前所未有的机遇: 2010年以来, 海气通量驱动的全球海洋环流高分辨率模拟和引潮力驱动的全球海洋潮汐高分辨率模拟逐渐合流, 海洋平衡运动和非平衡运动得以耦合于统一框架下[2~12]; 2022年发射的宽刈幅卫星高度

引用格式: 王传印, 刘志宇, 林宏阳, 等. 海洋多尺度动力分解新理论与方法. 科学通报, 2026, 71: 7314–7324
Wang C, Liu Z, Lin H, et al. New theory and technique for the dynamical decomposition of multiscale oceanic motions (in Chinese). Chin Sci Bull, 2026, 71: 7314–7324, doi: 10.1360/CSB-2025-5574

© 2025《中国科学》杂志社

计Surface Water and Ocean Topography(SWOT), 首次实现了在全球范围内对海面多尺度动力过程的空间二维观测[13], 而2023年启动的智能敏捷海洋立体观测系统研发计划, 则有望在观测现场高效捕捉多尺度动力过程的空间三维结构[14]. 实现上述不同场景下海洋平衡运动和非平衡运动的准确分离, 是揭示多尺度运动物理特征、阐明多尺度相互作用机理、发展满足能量守恒约束海洋数值模型的关键. 因此, 多尺度运动分解(即将全流分解为平衡运动和非平衡运动)逐渐成为了海洋多尺度动力学研究的焦点[15~18]. 过去几年, 我们发展了适用于上述不同应用场景的海洋多尺度运动动力分解理论与方法[19~22]. 本文旨在对这些理论和方法进行简要总结, 以期推动它们在海洋多尺度相互作用与能量串级机理及相关研究领域的应用.

1 面向高分辨率数值模拟数据应用的动力分解理论与方法

1.1 已有分解方案概述

以MITgcm LLC4320[11,12]为代表的全球潮分辨(tide-resolving)、亚中尺度相容(submesoscale-admitting)数值模拟旨在全面勾勒大尺度环流、正压潮、中尺度流动、内波、亚中尺度运动等多时空尺度动力过程. 面向该类高分辨率模拟数据应用的分解方案一般充分利用海水运动的时间演化规律, 因此要求海水运动物理场足够高频(如: 逐小时海面高度场). 这类分解方案主要包括时间滤波[23~25]、时空滤波[26,27]、拉格朗日滤波[18,28]等. 例如, 时间滤波将全流的低通、带通、高通部分分别对应为中尺度流动、亚中尺度运动和内波[23]; 时空滤波从海面流速或海面高度的频率-波数谱出发, 操作性地将全日潮频率和第十模态内波频散关系作为截止频率-波数线, 定义频率高于截止频率-波数线的运动为非平衡运动、频率低于截止频率-波数线的运动为平衡运动[26]; 拉格朗日滤波考虑了背景流造成的多普勒频移效应, 将全流坐标系下的超惯性频段运动视为非平衡运动, 将亚惯性频段运动视为平衡运动[18]. 然而, 时间滤波、时空滤波和拉格朗日滤波给出的平衡运动和非平衡运动之间存在明显重叠[19,20,29], 亟需发展尽可能准确将两类运动分离的普适性方法.

1.2 动力分解理论与方法介绍

一方面, 我们根据不同类型运动在谱空间(即经傅里叶变换后的频率-波数空间; 图1)的动力属性, 将海水运动物理场分解为大尺度环流、正压潮、低模态内波、中尺度流动、高模态内波和亚中尺度运动等六类典型过程[19]. 以南海中部~8°×5°海域的LLC4320模拟结果为例, 可将该动力分解方法的主要思想概括如下:

提取大尺度环流和正压潮. 大尺度环流和正压潮的水平尺度为$O(10^3)$公里, 在谱空间占据近零波数部分, 故而可通过提取空间线性趋势获得; 大尺度环流和正压潮分属亚惯性运动和超惯性运动, 可通过简单的时域滤波或潮汐调和分析进一步分离. 图2(a, d)分别展示了南海中部海域大尺度环流和正压潮对应的海面高度, 可清晰看出两类运动的大尺度特征.

提取低模态内波. 定义第一、二斜压模态内波为低模态内波. 低模态内波强烈受制于频散关系, 可通过包络第一、二模态内波频散关系的窄波数段(图1中黑线)提取. 图2(b)展示了南海中部海域低模态内波对应的海面高度, 其最显著的特征是西南向传播的规则波纹状结构.

提取中尺度运动. 扣除大尺度环流后, 中尺度运动在频率-波数谱图中占据低频、低波数空间, 可通过时间低通、空间低通滤波提取. 截止周期和波长可分别设定为研究海域惯性周期的最大值和第一斜压罗斯贝变形半径的最小值. 就所选南海中部海域而言, 截止周期和波长分别为46.2 h(图1中粉红色横线)和50 km(图1中粉红色竖线). 图2(e)展示了中尺度海面高度, 气旋和反气旋涡是其主要特征.

提取高模态内波和亚中尺度运动. 定义第三和更高模态内波为高模态内波. 高模态内波和亚中尺度运动在时空域存在显著重叠[30], 无法通过类似低模态内波的提取方式获得; 实际上, 分离高模态内波和亚中尺度运动是学界公认的难题[30]. 我们通过类比线性化控制方程中平衡模态和非平衡模态经典理论发现, 利用谱空间相对涡度(特指相对涡度矢量的垂向分量)和水平散度(特指水平速度的散度)的相对大小可实现两类运动的有效分离: 高模态内波水平散度的模大于相对涡度的模, 亚中尺度运动水平散度的模则小于相对涡度的模. 图2(c, f)分别展示了高模态内波和亚中尺度运动对应的海面高度. 高模态内波呈现出与低模态内波类似的波纹状结构, 只是空间尺度小很多; 亚中尺度海面高度则以较小尺度涡旋和带状丝形结构为主.

另一方面, 我们通过考虑大尺度背景流的平流作用, 推广了平衡模态与非平衡模态的经典理论, 发展了

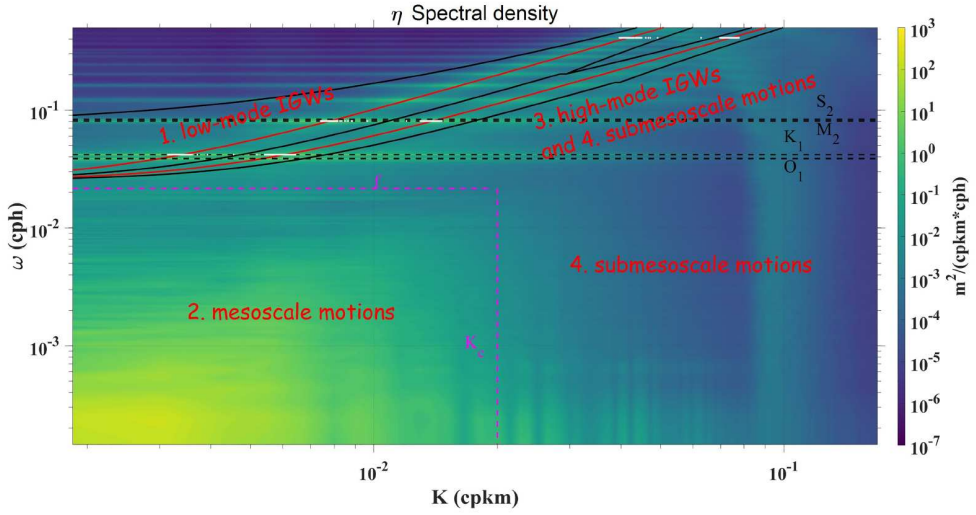


图 1 南海中部海域海面高度的频率-波数谱[19]. 红色实线表示第一、二斜压模态内波的频散关系. 黑色实线表示包络第一、二模态内波频散关系的窄波数段. 黑色虚线表示主要潮频率(K_1、O_1、M_2、S_2). 粉红色水平虚线表示低模态内波与中尺度运动之间的截止频率(即研究海域最小惯性频率). 粉红色垂向虚线表示中尺度运动与亚中尺度运动之间的截至波数(即研究海域第一斜压罗斯贝变形半径的最小值). 图中也标注了低模态内波(1)、中尺度运动(2)、高模态内波(3)、亚中尺度运动(4). Copyright © 2023 American Geophysical Union

Figure 1 Frequency-wavenumber spectrum of the sea surface height in the central South China Sea[19]. The solid red curves depict dispersion relations for mode-1 and mode-2 internal gravity waves. The solid black curves surrounding them delimit what is defined as low-mode internal gravity waves. The dashed black lines indicate the major tidal frequencies (K_1, O_1, M_2, S_2). The horizontal dashed magenta line represents the cutoff frequency (i.e., the inertial frequency at the southern edge of the study region) between low-mode IGWs and mesoscale motions. The vertical dashed magenta line marks the cutoff wavenumber (i.e., corresponding to the minima of the first baroclinic deformation radii in the study region) between mesoscale and submesoscale motions. Also defined and labeled are low-mode internal gravity waves (1), mesoscale motions (2), high-mode internal gravity waves (3), and submesoscale motions (4). Copyright © 2023 American Geophysical Union

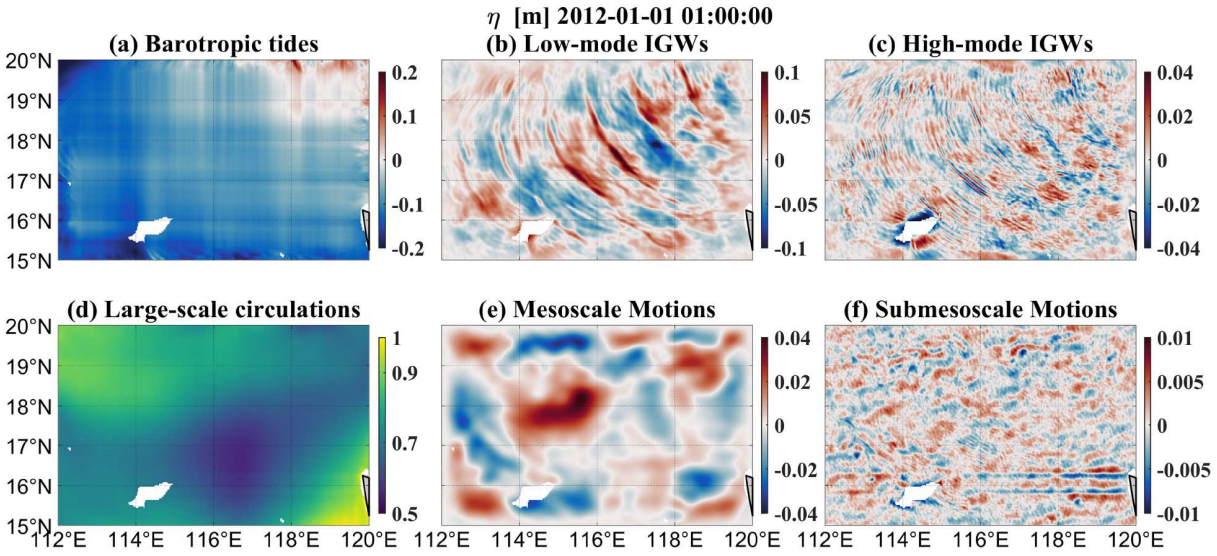


图 2 南海中部海域正压潮(a)、低模态内波(b)、高模态内波(c)、大尺度流动(d)、中尺度流动(e)和亚中尺度运动(f)对应的海面高度

Figure 2 Sea surface height corresponding to barotropic tides (a), low-mode IGWs (b), high-mode IGWs (c), large-scale circulations (d), mesoscale motions (e) and submesoscale motions (f) in the central South China Sea

将海水运动物理场分解为平衡运动和非平衡运动的方法, 对应推导出了两类运动的控制方程, 建立了量化两类运动相互作用的理论框架[20]. 该动力分解方法的主要思想可概括如下:

动力分解滤波器的构建. 考虑大尺度背景流的平流效应, 控制海水运动的线性化相对涡度方程可表示为

$$\frac{\partial\zeta}{\partial t}+U\frac{\partial\zeta}{\partial x}+V\frac{\partial\zeta}{\partial y}+f_{\min}\frac{f\chi}{f_{\min}}=0, \tag{1}$$

其中U、V表示背景流且不随时间、空间变化, $\zeta=\frac{\partial v}{\partial x}-\frac{\partial u}{\partial y}$表示全流的相对涡度, $\chi=\frac{\partial u}{\partial x}+\frac{\partial v}{\partial y}$表示全流的水平散度, f=f_0+βy表示β平面近似下的科氏参数, $f_{\min}$表示研究海域最南端(即最小)的科氏参数. 式(1)中通过引入$f_{\min}$定义了修正的水平散度($\frac{f\chi}{f_{\min}}$), 目的是将科氏参数随纬度的变化合并到水平散度中. 对式(1)进行傅里叶变换得:

$$i\omega\widehat{\zeta}+ikU\widehat{\zeta}+ilV\widehat{\zeta}+f_{\min}\frac{\widehat{f\chi}}{f_{\min}}=i\Omega\widehat{\zeta}+f_{\min}\frac{\widehat{f\chi}}{f_{\min}}=0, \tag{2}$$

其中^代表傅里叶变换后的变量, ω、k、l分别表示绝对频率、东西向波数和南北向波数, Ω=ω+kU+lV表示固有频率. 由式(2)出发, 借鉴经典(非)平衡模态理论, 定义如下动力分解滤波器:

$$\widehat{M}(k,l,\omega)=\begin{cases}0, \text{if}\left(|\widehat{\zeta}|<\left|\frac{\widehat{f\chi}}{f_{\min}}\right| \text{ and } |\omega|>|f_{\min}|\right) \text{at } (k,l,\omega)\\ 1, \text{if}\left(|\widehat{\zeta}|>\left|\frac{\widehat{f\chi}}{f_{\min}}\right| \text{ or } |\omega|<|f_{\min}|\right) \text{at } (k,l,\omega)\end{cases}, \tag{3}$$

$$\widehat{\overline{M}}(k,l,\omega)=\begin{cases}1, \text{if}\left(|\widehat{\zeta}|<\left|\frac{\widehat{f\chi}}{f_{\min}}\right| \text{ and } |\omega|>|f_{\min}|\right) \text{at } (k,l,\omega)\\ 0, \text{if}\left(|\widehat{\zeta}|>\left|\frac{\widehat{f\chi}}{f_{\min}}\right| \text{ or } |\omega|<|f_{\min}|\right) \text{at } (k,l,\omega)\end{cases}, \tag{4}$$

其中, ¯和˜分别表示平衡运动和非平衡运动, $\overline{M}(x,y,t)$和$\widetilde{M}(x,y,t)$分别表示物理空间中平衡运动和非平衡运动的滤波器.

全流控制方程的动力分解. 定义动力分解滤波器后, 可对任一物理场A作如下分解:

$$\begin{cases}\widehat{\overline{A}}(k,l,\omega)=\widehat{\overline{M}}\cdot\widehat{A}\\ \widehat{\widetilde{A}}(k,l,\omega)=\widehat{\overline{M}}\cdot\widehat{A}\end{cases}, \tag{5}$$

$$\begin{cases}\overline{A}=\overline{M}*A\\ \quad=\iiint\overline{M}(\tau_x,\tau_y,\tau_t)\cdot A(x-\tau_x,y-\tau_y,t-\tau_t)\mathrm{d}\tau_x\mathrm{d}\tau_y\mathrm{d}\tau_t\\ \widetilde{A}=\widetilde{M}*A\\ \quad=\iiint\widetilde{M}(\tau_x,\tau_y,\tau_t)\cdot A(x-\tau_x,y-\tau_y,t-\tau_t)\mathrm{d}\tau_x\mathrm{d}\tau_y\mathrm{d}\tau_t\end{cases}, \tag{6}$$

其中, •表示乘号, *表示卷积. 对海水运动控制方程卷积平衡运动滤波器$\overline{M}$, 利用卷积和微分可以交换顺序的性质, 即可得到平衡运动的控制方程

$$\begin{cases}\frac{\partial\overline{u}}{\partial t}+\frac{\partial\overline{uu}}{\partial x}+\frac{\partial\overline{vu}}{\partial y}+\frac{\partial\overline{wu}}{\partial z}-\overline{fv}=-\frac{1}{\rho_0}\frac{\partial\overline{p}}{\partial x}+\overline{S_u}\\ \frac{\partial\overline{v}}{\partial t}+\frac{\partial\overline{uv}}{\partial x}+\frac{\partial\overline{vv}}{\partial y}+\frac{\partial\overline{wv}}{\partial z}+\overline{fu}=-\frac{1}{\rho_0}\frac{\partial\overline{p}}{\partial y}+\overline{S_v}\\ \frac{\partial\overline{p}}{\partial z}=-\rho g\\ \frac{\partial\overline{u}}{\partial x}+\frac{\partial\overline{v}}{\partial y}+\frac{\partial\overline{w}}{\partial z}=0\\ \frac{\partial\overline{\rho}}{\partial t}+\frac{\partial\overline{u\rho}}{\partial x}+\frac{\partial\overline{v\rho}}{\partial y}+\frac{\partial\overline{w\rho}}{\partial z}-\frac{\rho_0}{g}\overline{wN^2}=\overline{S_\rho}\end{cases}, \tag{7}$$

其中, p表示压强扰动, ρ_0表示参考密度, ρ表示密度扰动, S_u、S_v和S_ρ分别表示东西向动量方程、南北向动量方程和密度方程中的源汇项, g表示重力加速度, N表示背景浮性频率. 通过类似的方式可推导出非平衡运动的控制方程.

作为应用示例, 图3和4分别展示了LLC4320南海中部海域非平衡运动和平衡运动东西向动量方程中各项的空间分布. 整体而言, 局地导数、科氏力和压强梯度力主导着非平衡运动动量的演化. 比较而言, 平衡运动主要受科氏力和压强梯度力(即地转平衡)控制. 需要指出的是, 平衡运动压强梯度力(图4(e))和源汇项(图4(f))中的波纹状条形结构是由傅里叶变换所致的吉布斯现象, 本文结论部分将会对该现象作进一步说明.

2 面向SWOT宽刈幅卫星数据应用的动力分解方法

2.1 已有分解方案概述

以SWOT为代表的宽刈幅卫星高度计首次从观测角度揭示了全球海洋大尺度环流、中尺度流动、亚中尺度过程等平衡运动和正压潮、内波等非平衡运动的精细化面貌. 然而, 宽刈幅卫星的重复观测周期过长(1

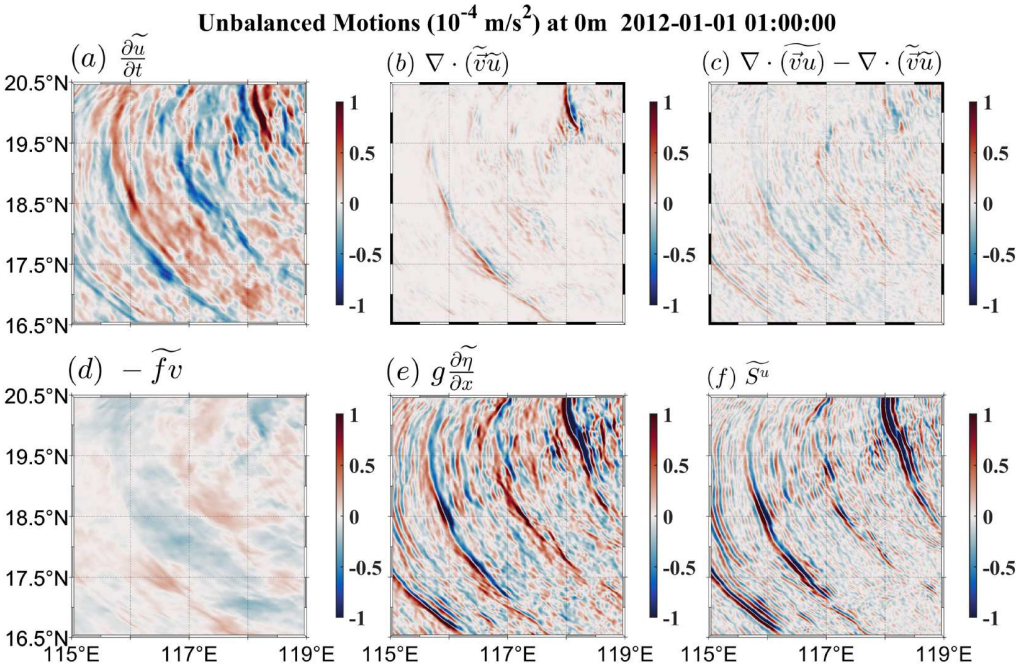


图 3 南海中部海域非平衡运动东西向动量方程中各项的空间分布[20]. (a) 局地导数; (b) 自身的相互作用; (c) 与平衡运动的相互作用; (d) 科氏力; (e) 压强梯度项; (f) 源汇项. Copyright © 2023, American Meteorological Society

Figure 3 Individual terms of the zonal momentum equation governing the unbalanced motions in the central South China Sea[20]. (a) The time derivative; (b) self-interaction term; (c) interaction with the balanced motions; (d) Coriolis term; (e) pressure gradient term; (f) source/sink term. Copyright © 2023, American Meteorological Society

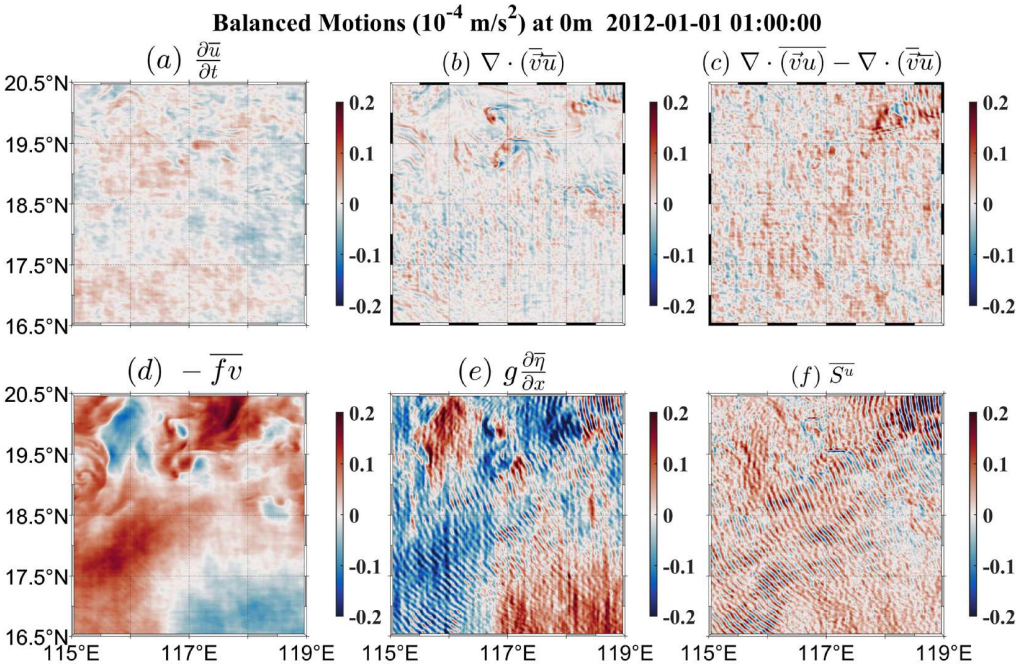


图 4 南海中部海域平衡运动东西向动量方程中各项的空间分布[20]. (a) 局地导数; (b) 自身的相互作用; (c) 与非平衡运动的相互作用; (d) 科氏力; (e) 压强梯度项; (f) 源汇项. Copyright © 2023, American Meteorological Society

Figure 4 Individual terms of the zonal momentum equation governing the balanced motions in the central South China Sea[20]. (a) The time derivative; (b) self-interaction term; (c) interaction with the unbalanced motions; (d) Coriolis term; (e) pressure gradient term; (f) source/sink term. Copyright © 2023, American Meteorological Society

或21天), 观测数据存在显著的时域不连续性, 致使基于该类观测数据的平衡运动和非平衡运动的分离颇具挑战性[31,32]. 相关的研究较少, 主要分为直接基于宽刈幅卫星数据的研究和基于数值模拟的概念验证(proof-of-concept)研究. 前者包括: 利用潮汐调和分析或平面波拟合提取SWOT数据中的相干内潮信号[33,34], 该方法不适用于非相干内潮和非潮频内波的提取; 利用动力模态分解从SWOT数据中提取地转运动[35], 该方法为平衡运动和非平衡运动的分离提供了新视角, 值得深入的研究以探索其普适性. 后者包括: 把海面高度波数谱斜率的不连续点作为截止波数, 对海面高度进行空间低通滤波得到平衡运动、高通滤波得到非平衡运动, 该分解方案只适用于夏季[36]; 将海面高度数据同化至海洋数值模式中, 再利用模式模拟结果分离平衡运动和非平衡运动[37,38]; 利用额外引入的海面密度场估算位势涡度场, 然后反解准地转位势涡度得出平衡运动的海面高度, 将全流海面高度与平衡运动海面高度之差视作非平衡运动海面高度[39]; 机器学习在多尺度运动分解方面也展现出一定的潜力[40~42]; 这类概念验证研究的共性问题是研究结论在实际海洋中的适用性尚不清晰. 综合来看, 面向SWOT宽刈幅卫星数据应用的分解研究还处在起步阶段, 已有的分解方案也缺乏普适性, 需探索普适、高效的分解方案.

2.2 动力分解方法介绍

近期, 我们通过额外引进海表面流场数据, 参照数值天气预报中初始化问题的解决思路, 实现了瞬时海面高度场的动力分解[21,22]. 该动力分解方法的数学表达可总结如下:

$$\begin{cases} \nabla^2\left(\dfrac{g\bar{\eta}}{f_0}\right)-\dfrac{1}{L_d^2}\dfrac{g\bar{\eta}}{f_0}=\Pi=\zeta-\dfrac{1}{L_d^2}\dfrac{g\eta}{f_0} \\ f_0\times\bar{\boldsymbol{u}}=-g\nabla\bar{\eta} \\ \tilde{\eta}=\eta-\bar{\eta} \\ \tilde{\boldsymbol{u}}=\boldsymbol{u}-\bar{\boldsymbol{u}} \end{cases}, \tag{8}$$

其中$\boldsymbol{u}=(u,\ v)$表示海表流速, η表示海面高度, $\Pi=\zeta-\dfrac{1}{L_d^2}\dfrac{g\eta}{f_0}$表示线性化的位势涡度异常, $f_0=(0,\ 0,\ \mathrm{f}_0)$, L_d表示罗斯贝变形半径. 该动力分解方法的核心思想包括两点: (1) 非平衡运动不携带位势涡度异常[43,44], 亦即所有的位势涡度异常均由平衡运动所致, 式(8)中第一个等式正是该思想的数学表达; (2) L_d是综合考虑所有垂向斜压模态的有效罗斯贝变形而非对应经典浅水方程系统里的单一模态[21,36,37].

作为应用示例, 首先我们将式(8)应用于南海中部

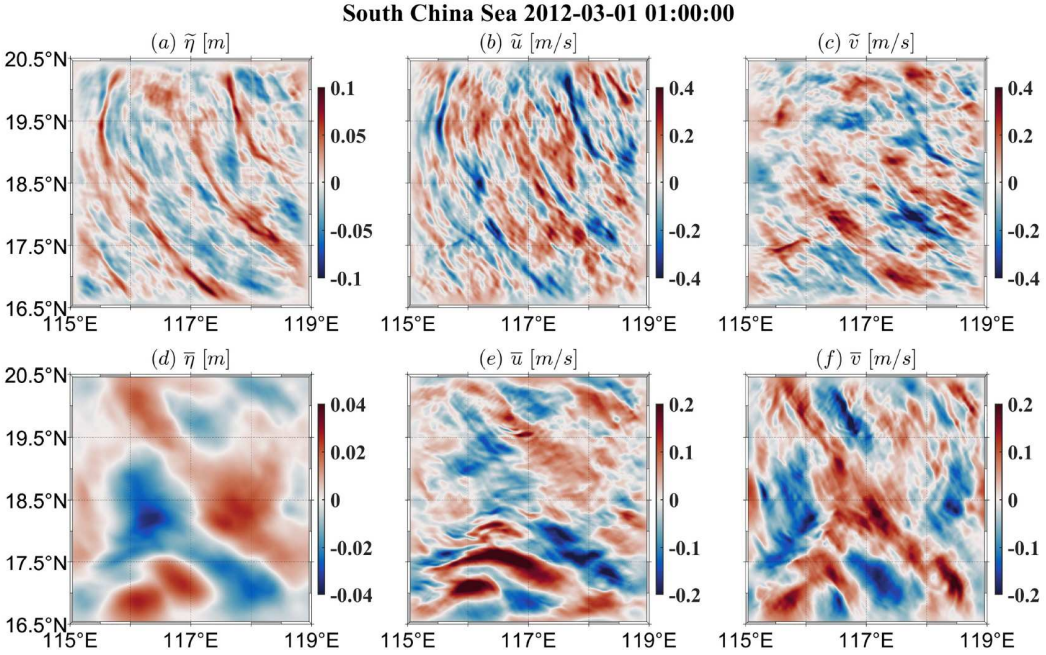


图 5 基于高分辨率数值模拟数据分解的南海中部海域海面高度(a, d)、东西向流速(b, e)及南北向流速(c, f)[21]. 第一(a~c)、二行(d~f)分别表示非平衡运动和平衡运动. Copyright © 2025, Elsevier

Figure 5 The decomposed sea surface height (a, d), zonal velocity (b, e) and meridional velocity (c, f) based on a high-resolution numerical simulation of the central South China Sea[21]. The upper (a–c) and lower (d–f) panels represent unbalanced and balanced motions, respectively. Copyright © 2025, Elsevier

海域的LLC4320模拟数据，分解结果见图5. 非平衡运动对应的海面高度(图5(a))和流速(图5(b, c))显著呈现出西南向传播的内波信号，平衡运动物理量(图5(d~f))则以中尺度流动为主，同时也包含亚中尺度过程信号，这些亚中尺度信号在流速上体现得尤为明显. 其次，将式(8)应用于实际海洋观测数据. 加州外海密布着观测海表面流速的高频地波雷达网，可与SWOT轨道进行很好的匹配，因此该海域非常适合作为动力分解即式(8)的应用示范，相关的分解结果见图6. 与南海不同的是，该海域的非平衡运动呈现不规则分布(图6(a~c)). 与南海类似的是，中尺度信号主导加州外海的平衡运动(图6(d~f)).

3 总结与展望

本文扼要回顾了过去几年我们在海洋多尺度运动分解方面进行的探索. 面向高分辨率模拟数据的应用，我们利用不同动力过程物理属性的差异提出了连续时间物理场中平衡运动与非平衡运动的动力分解方法，并导出了两类运动的控制方程；面向SWOT宽刈幅海面高度数据的应用，我们利用内波不携带位势涡度异

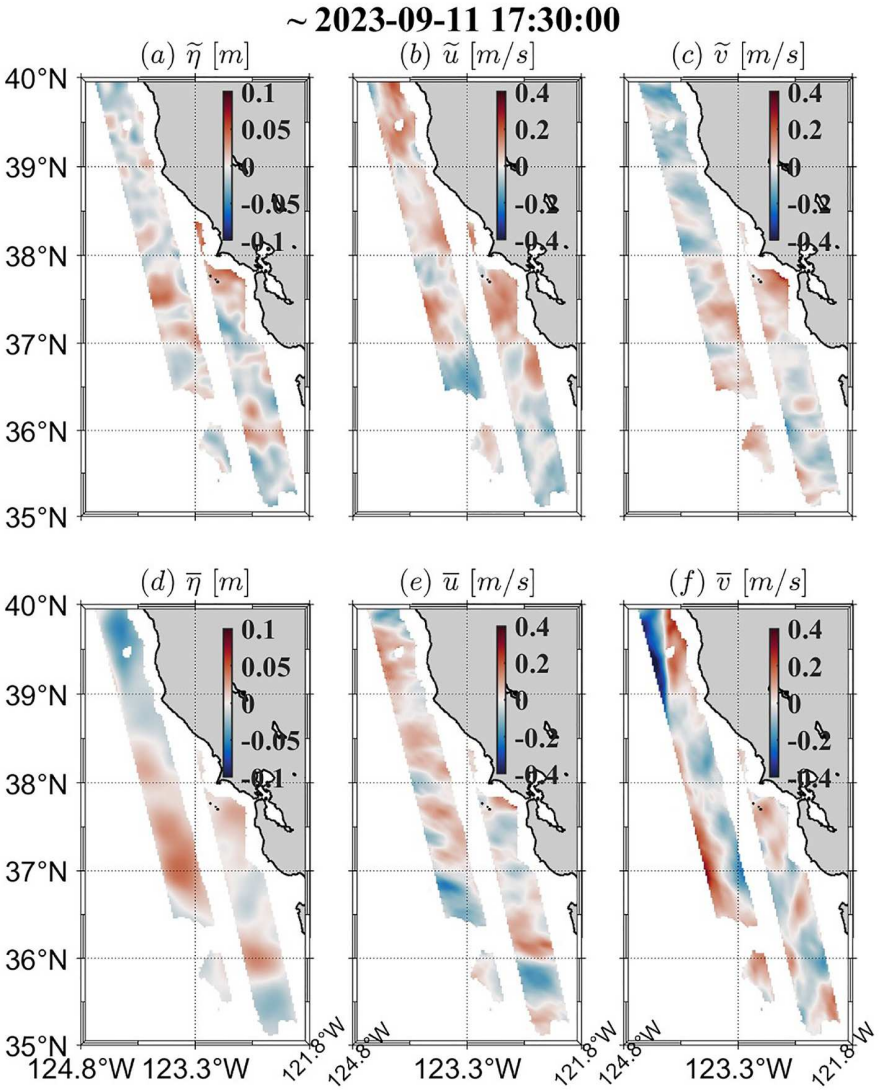


图 6 基于SWOT/高频地波雷达观测数据分解的加州外海海面高度(a, d)、东西向流速(b, e)及南北向流速(c, f)[22]. 第一(a~c)、二行(d~f)分别表示非平衡运动和平衡运动. Copyright © 2025, American Geophysical Union

Figure 6 The decomposed sea surface height (a, d), zonal velocity (b, e) and meridional velocity (c, f) based on Surface Water and Ocean Topography/high–frequency radar measurements offshore of California[22]. The upper (a–c) and lower (d–f) panels represent unbalanced and balanced motions, respectively. Copyright © 2025, American Geophysical Union

常这一基本动力学性质，建立了由海面高度场中分离出平衡运动与非平衡运动的方法．利用高分辨率数值模拟数据和实际海洋观测数据，在南海和加州外海对上述动力分解方法进行了应用示例研究，分解出的平衡运动和非平衡运动揭示了各自应有的物理特征，这显示了本文动力分解方法的有效性与实用性．将动力分解与传统时空尺度分解相结合，可望显著推动海洋多尺度耦合与能量传递机理研究．

鉴于海洋平衡运动和非平衡运动的分离是一项极具挑战性的课题，我们的研究应被视为实现更准确分离道路上的初步探索．因此，需要清晰阐述动力分解方法的局限性，并明确未来研究的改进方向．首先，面向高分辨率模拟数据应用的动力分解方案采用的0/1型滤波器(即式(3)和(4))会引发吉布斯现象．由于动力分解滤波器中0/1分布的复杂性，简单低通或高通滤波中用于缓解吉布斯现象的常规方法(即使滤波器值从1到0连续衰减)似乎不适用于式(3)和(4)，需要探索更简单有效的方式．其次，面向SWOT宽刈幅数据应用的动力分解主要适用于小罗斯贝数、小弗劳德数、平衡运动和非平衡运动量级相当的动力环境；为了拓广适用范围，未来的研究可考虑借鉴数值天气预报中初始化问题更高阶的处理方法，例如：非线性标准模初始化[45~47]、数字滤波[48,49]、带高阶修正的准地转理论[50~53]、最优位势涡度平衡[54]以及最优平衡法[55~57]．最后，由于赤道海域动力过程的独特性，两类动力分解均不适用于该海域．在未来的研究中，我们将致力于解决上述问题，发展更具鲁棒性与普适性的动力分解理论与方法．

参考文献

1 Research Group for the “Study of Development Strategies for Disciplines and Frontier Fields in China (2021–2035)”. China’s Ocean Science Development Strategy by 2035 (in Chinese). Beijing: Science Press, 2023 [“中国学科及前沿领域发展战略研究(2021—2035)”项目组. 中国海洋科学2035发展战略. 北京: 科学出版社, 2023]

2 Arbic B K, Wallcraft A J, Metzger E J. Concurrent simulation of the eddying general circulation and tides in a global ocean model. Ocean Model, 2010, 32: 175–187

3 Arbic B, Richman J, Shriver J, et al. Global modeling of internal tides within an eddying ocean general circulation model. Oceanography, 2012, 25: 20–29

4 Fu H, Wu X, Li W, et al. Improving the accuracy of barotropic and internal tides embedded in a high-resolution global ocean circulation model of MITgcm. Ocean Model, 2021, 162: 101809

5 Arbic B, Alford M, Ansong J, et al. A primer on global internal tide and internal gravity wave continuum modeling in HYCOM and MITgcm. New Front Oper Oceanogr, 2018, 16: 307–309

6 Arbic B K. Incorporating tides and internal gravity waves within global ocean general circulation models: a review. Prog Oceanogr, 2022, 206: 102824

7 Müller M, Cherniawsky J Y, Foreman M G G, et al. Global M_2 internal tide and its seasonal variability from high resolution ocean circulation and tide modeling. Geophys Res Lett, 2012, 39: 2012GL053320

8 Müller M, Cherniawsky J Y, Foreman M G G, et al. Seasonal variation of the M_2 tide. Ocean Dyn, 2014, 64: 159–177

9 Li Z, Storch J S, Müller M. The M_2 internal tide simulated by a 1/10° OGCM. J Phys Oceanogr, 2015, 45: 3119–3135

10 Waterhouse A F, MacKinnon J A, Nash J D, et al. Global patterns of diapycnal mixing from measurements of the turbulent dissipation rate. J Phys Oceanogr, 2014, 44: 1854–1872

11 Rocha C B, Gille S T, Chereskin T K, et al. Seasonality of submesoscale dynamics in the Kuroshio Extension. Geophys Res Lett, 2016, 43: 11–304

12 Rocha C B, Chereskin T K, Gille S T, et al. Mesoscale to submesoscale wavenumber spectra in Drake Passage. J Phys Oceanogr, 2016, 46: 601–620

13 Fu L, Pavelsky T, Cretaux J, et al. The surface water and ocean topography mission: a breakthrough in radar remote sensing of the ocean and land surface water. Geophys Res Lett, 2024, 51: e2023GL107652

14 Dong C, Chen D, Wang D, et al. Intelligent swift ocean observing system. Ocean-Land-Atmos Res, 2023, 2: 0022

15 Bühler O, Callies J, Ferrari R. Wave–vortex decomposition of one-dimensional ship-track data. J Fluid Mech, 2014, 756: 1007–1026

16 Bühler O, Kuang M, Tabak E G. Anisotropic Helmholtz and wave–vortex decomposition of one-dimensional spectra. J Fluid Mech, 2017, 815: 361–387

17 Wang H, Bühler O. Ageostrophic corrections for power spectra and wave–vortex decomposition. J Fluid Mech, 2020, 882: A16

18 Shakespeare C J, Gibson A H, Hogg A M C, et al. A new open source implementation of Lagrangian filtering: a method to identify internal waves

in high-resolution simulations. J Adv Model Earth Syst, 2021, 13: e2021MS002616
19 Wang C, Liu Z, Lin H. On dynamical decomposition of multiscale oceanic motions. J Adv Model Earth Syst, 2023, 15: e2022MS003556
20 Wang C, Liu Z, Lin H. A simple approach for disentangling vortical and wavy motions of oceanic flows. J Phys Oceanogr, 2023, 53: 1237–1249
21 Wang C, Liu Z, Lin H, et al. Disentangling wavy and vortical motions in concurrent snapshots of the sea surface height and velocity. Ocean Model, 2025, 196: 102556
22 Wang C, Liu Z, Lin H, et al. A practical separation of oceanic vortical and wavy motions entangled in the SWOT measurements. Geophys Res Lett, 2025, 52: e2024GL113995
23 Barkan R, Winters K B, McWilliams J C. Stimulated imbalance and the enhancement of eddy kinetic energy dissipation by internal waves. J Phys Oceanogr, 2017, 47: 181–198
24 Barkan R, Srinivasan K, Yang L, et al. Oceanic mesoscale eddy depletion catalyzed by internal waves. Geophys Res Lett, 2021, 48: 1
25 Garabato A C N, Yu X, Callies J, et al. Kinetic energy transfers between mesoscale and submesoscale motions in the open ocean's upper layers. J Phys Oceanogr, 2022, 52: 75–97
26 Qiu B, Chen S, Klein P, et al. Seasonality in transition scale from balanced to unbalanced motions in the world ocean. J Phys Oceanogr, 2018, 48: 591–605
27 Torres H S, Klein P, Menemenlis D, et al. Partitioning ocean motions into balanced motions and internal gravity waves: a modeling study in anticipation of future space missions. J Geophys Res Oceans, 2018, 123: 8084–8105
28 Nagai T, Tandon A, Kunze E, et al. Spontaneous generation of near-inertial waves by the Kuroshio front. J Phys Oceanogr, 2015, 45: 2381–2406
29 Jones C S, Xiao Q, Abernathey R P, et al. Using Lagrangian filtering to remove waves from the ocean surface velocity field. J Adv Model Earth Syst, 2023, 15: e2022MS003220
30 McWilliams J. Submesoscale currents in the ocean. Proc R Soc A Math Phys Eng Sci, 2016, 472
31 Morrow R, Fu L L, Ardhuin F, et al. Global observations of fine-scale ocean surface topography with the surface water and ocean topography (SWOT) mission. Front Mar Sci, 2019, 6: 1–9
32 Archer M, Wang J, Klein P, et al. Wide-swath satellite altimetry unveils global submesoscale ocean dynamics. Nature, 2025, 640: 691–696
33 Tchilibou M, Carrere L, Lyard F, et al. Internal tides off the Amazon shelf in the western tropical Atlantic: analysis of SWOT Cal/Val mission data. Ocean Sci, 2025, 21: 325–342
34 Zhao Z. Internal tides from SWOT: a 75-day instantaneous mode-1 M_2 internal tide model. J Geophys Res Oceans, 2024, 129: e2024JC021174
35 Uchida T, Yadidya B, Lapo K E, et al. Dynamic mode decomposition of geostrophically balanced motions from SWOT Cal/Val in the separated Gulf Stream. Earth Space Sci, 2025, 12: e2024EA004079
36 Torres H S, Klein P, Siegelman L, et al. Diagnosing ocean-wave-turbulence interactions from space. Geophys Res Lett, 2019, 46: 8933–8942
37 Le Guillou F, Lahaye N, Ubelmann C, et al. Joint estimation of balanced motions and internal tides from future wide-swath altimetry. J Adv Model Earth Syst, 2021, 13: 1–17
38 Yadidya B, Arbic B K, Shriver J F, et al. Phase-accurate internal tides in a global ocean forecast model: potential applications for nadir and wide-swath altimetry. Geophys Res Lett, 2024, 51: e2023GL107232
39 Ponte A L, Klein P, Dunphy M, et al. Low-mode internal tides and balanced dynamics disentanglement in altimetric observations: synergy with surface density observations. J Geophys Res Oceans, 2017, 122: 2143–2155
40 Wang H, Grisouard N, Salehipour H, et al. A deep learning approach to extract internal tides scattered by geostrophic turbulence. Geophys Res Lett, 2022, 49: 1–9
41 Gao Z, Chapron B, Ma C, et al. A deep learning approach to extract balanced motions from sea surface height snapshot. Geophys Res Lett, 2024, 51: e2023GL106623
42 Lguensat R, Fablet R, Le Sommer J, et al. Filtering internal tides from wide-swath altimeter data using convolutional neural networks. IGARSS 2020–2020 IEEE International Geoscience and Remote Sensing Symposium, Waikoloa, HI, USA, 2020. 3904–3907
43 Pedlosky J. Waves in the Ocean and Atmosphere. Berlin, Heidelberg: Springer, 2003
44 Zeitlin V. Geophysical Fluid Dynamics: Understanding (Almost) Everything with Rotating Shallow Water Models. Oxford: Oxford University Press, 2018
45 Baer F, Tribbia J J. On complete filtering of gravity modes through nonlinear initialization. Mon Wea Rev, 1977, 105: 1536–1539
46 Machenhauer B. On the dynamics of gravity oscillations in a shallow water model, with application to normal mode initialization. Beitr Phys Atmos, 1977, 50: 253–271
47 Chouksey M, Eden C, Brüggemann N. Internal gravity wave emission in different dynamical regimes. J Phys Oceanogr, 2018, 48: 1709–1730
48 Lynch P, Giard D, Ivanovici V. Improving the efficiency of a digital filtering scheme for diabatic initialization. Mon Wea Rev, 1997, 125: 1976–1982
49 Lynch P, Huang X Y. Initialization of the HIRLAM model using a digital filter. Mon Wea Rev, 1992, 120: 1019–1034

50 Dù R, Smith K. Emergent vorticity asymmetry of one and two-layer shallow water system captured by a next-order balanced model. arXiv: 2411.02291, 2024
51 Spall M A, Mcwilliams J C. Rotational and gravitational influences on the degree of balance in the shallow-water equations. Geophys Astrophys Fluid Dyn, 1992, 64: 1–29
52 Vallis G K. Potential vorticity inversion and balanced equations of motion for rotating and stratified flows. Quart J R Meteoro Soc, 1996, 122: 291–322
53 Warn T, Bokhove O, Shepherd T G, et al. Rossby number expansions, slaving principles, and balance dynamics. Quart J R Meteoro Soc, 1995, 121: 723–739
54 Viúdez Á, Dritschel D G. Optimal potential vorticity balance of geophysical flows. J Fluid Mech, 2004, 521: 343–352
55 Chouksey M, Eden C, Masur G T, et al. A comparison of methods to balance geophysical flows. J Fluid Mech, 2023, 971: 1–9
56 Masur G T, Oliver M. Optimal balance for rotating shallow water in primitive variables. Geophys Astrophys Fluid Dyn, 2020, 114: 429–452
57 Rosenau S, Chouksey M, Eden C. Towards realistic ocean flow decomposition using optimal balance with time-averaging. arXiv: 2501.11464, 2025

Summary for “海洋多尺度动力分解新理论与方法”

New theory and technique for the dynamical decomposition of multiscale oceanic motions

Chuanyin Wang[1], Zhiyu Liu[2*], Hongyang Lin[2], Qinghua Yang[1,3], Qinbiao Ni[1] & Dake Chen[1,4]

[1] *Southern Marine Science and Engineering Guangdong Laboratory (Zhuhai), Zhuhai 519082, China*
[2] *State Key Laboratory of Marine Environmental Science, College of Ocean and Earth Sciences, Xiamen University, Xiamen 361102, China*
[3] *School of Atmospheric Sciences, Sun Yat-sen University, Zhuhai 519082, China*
[4] *State Key Laboratory of Satellite Ocean Environment Dynamics, Second Institute of Oceanography, Ministry of Natural Resources, Hangzhou 310012, China*
* Corresponding author, E-mail: zyliu@xmu.edu.cn

Oceanic motions are characterized by a variety of dynamical regimes, with each regime encompassing multiple spatiotemporal scales. The multiscale interaction among those dynamical regimes is a major research frontier in the realm of physical oceanography. The decomposition of the oceanic motions is crucial to exploring the multiscale interaction and quantifying the cross-scale energy transfer. Currently, the widely used decomposition approaches are essentially the space/time scale separations and thus are incapable of accurately separating physical processes with similar space/time scales but contrasting dynamics; this limitation hinders the advancement of multiscale ocean dynamics. Over the past few years, we have proposed several dynamical decomposition frameworks that aim at different application scenarios. Firstly, several global high-resolution simulations have recently begun to include astronomical tidal forcings in addition to atmospheric forcings and thus have the potential to reproduce multiple dynamical regimes in the ocean. A proper decomposition applicable to the temporally continuous output from such tide-resolving simulations remains a major difficulty. To address this difficulty, we devised two ideas. The first one is based on the respective dynamical characteristics of different dynamical regimes. Specifically, large-scale currents and barotropic tides have the largest horizontal scales but contrasting frequencies; low-mode internal gravity waves are well constrained by linear dispersion relations, whereas mesoscale flows are of relatively low frequency and with horizontal scales above the first baroclinic deformation radius; the intrinsic frequency of high-mode internal gravity waves is above the inertial frequency while the intrinsic frequency of submesoscale flows is well below the inertial frequency. Taking advantage of those characteristics, we were able to decompose a full flow into six prototypical oceanic flow regimes. For the second idea, we introduced a mean flow and extended the classic theory of balanced and unbalanced modes in geophysical fluid dynamics. The extended theory was then utilized to design a dynamical filter for disentangling the balanced (e.g., large-scale currents, mesoscale flows, submesoscale flows) and unbalanced (e.g., barotropic tides, internal gravity waves) motions, based on relative magnitudes of the relative vorticity and the horizontal divergence in spectral space. Correspondingly, the governing equations of the balanced and unbalanced motions were derived from the primitive equations of the full flow. The applications to model outputs from a realistic tide-resolving and submesoscale-admitting simulation showed that those two dynamical decompositions are simple and efficient. Secondly, the recently-launched Surface Water and Ocean Topography (SWOT) satellite provides an unprecedented two-dimensional measurement of the sea surface height down to the oceanic submesoscale of 1–10 km. The measured sea surface height by SWOT contains combined contributions of balanced and unbalanced motions. Separating their respective contributions is extremely challenging due to the long-repeat period (i.e., 1 day or 21 days) of the SWOT satellite. To achieve a practical separation, we adopted the linear normal-mode initialization technique used in numerical weather prediction. This technique is deeply rooted in geophysical fluid dynamics and exploits the basic property that unbalanced motions do not carry any potential vorticity anomaly. Relying on this initialization technique, we additionally introduced sea surface velocity data and developed an approach for decomposing a snapshot of sea surface height into balanced and unbalanced components. With concurrent measurements of sea surface height and velocity respectively from SWOT and the offshore high-frequency radar system, this separation method proves valid and useful. It is hoped that this series of dedicated efforts could lay the foundation for revealing the underlying mechanism of multiscale interaction in the simulation data and facilitating the scientific application of SWOT data.

dynamical decomposition, multiscale interaction, balanced motion, unbalanced motion, SWOT

doi: 10.1360/CSB-2025-5574